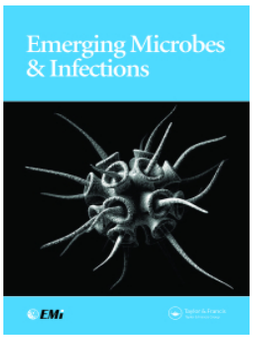

Emerging Microbes & Infections

ISSN: 2222-1751 (Online) Journal homepage: www.tandfonline.com/journals/temi20

Influenza NS1 drives N^6-methyladenosine (m^6A)-mediated autoregulation of viral mRNA splicing

Yingyin Liao, Jiayan Liu, Pui Wang, Bobo Wing-Yee Mok & Honglin Chen

To cite this article: Yingyin Liao, Jiayan Liu, Pui Wang, Bobo Wing-Yee Mok & Honglin Chen (2025) Influenza NS1 drives N^6-methyladenosine (m^6A)-mediated autoregulation of viral mRNA splicing, Emerging Microbes & Infections, 14:1, 2572761, DOI: 10.1080/22221751.2025.2572761

To link to this article: https://doi.org/10.1080/22221751.2025.2572761

Emerging Microbes & Infections
2025, VOL. 14, 2572761 (17 pages)
https://doi.org/10.1080/22221751.2025.2572761

Influenza NS1 drives N^6-methyladenosine (m^{6}A)-mediated autoregulation of viral mRNA splicing

Yingyin Liao[a,b,c], Jiayan Liu[a,b,c], Pui Wang[a,b], Bobo Wing-Yee Mok [a,b] and Honglin Chen [a,b,c]

[a]Department of Microbiology, Li Ka Shing Faculty of Medicine, The University of Hong Kong, Hong Kong Special Administrative Region, People's Republic of China; [b]State Key Laboratory for Emerging Infectious Diseases, The University of Hong Kong, Hong Kong Special Administrative Region, People's Republic of China; [c]Centre for Virology, Vaccinology and Therapeutics Limited, The University of Hong Kong, Hong Kong Special Administrative Region, People's Republic of China

ABSTRACT

Influenza A virus replication requires precise balance between unspliced and spliced viral mRNAs. However, the regulatory mechanisms governing viral mRNA splicing remain poorly understood. In this study, we uncover an epigenetic strategy whereby the viral NS1 protein autoregulates its own mRNA splicing via *N*^{6}-methyladenosine (m^{6}A) modification. Specifically, m^{6}A modification at residue A385 on NS mRNA recruits the m^{6}A reader YTHDC1, which competitively inhibits the splicing factor SRSF3 from binding proximal sites. Importantly, we demonstrate that the A385 m^{6}A site is conserved and essential for splicing regulation in the NS segment across human and avian influenza strains. Our findings suggest that, by dynamically modulating m^{6}A levels, NS1 fine-tunes viral mRNA processing to enhance replication efficiency. This work elucidates NS1 as an m^{6}A-driven splicing regulator and identifies this conserved m^{6}A site as a potential target for broad-spectrum antiviral development.

ARTICLE HISTORY Received 1 August 2025; Revised 27 September 2025; Accepted 4 October 2025

KEYWORDS Influenza virus; NS1; M^{6}A modification; viral mRNA splicing; epitranscriptomics

Introduction

More than one hundred different post-transcriptional modifications can be found in RNA across all living organisms, contributing to various biological functions such as RNA stability, splicing, translation, degradation and secondary structure [1–3]. By far, *N*^{6}-methyladenosine (m^{6}A) stands out as the most abundant among the post-transcriptional modifications [4]. The addition of m^{6}A modification is a dynamic process involving many m^{6}A-related proteins. Methyltransferase is a writer complex in which METTL3 is the catalytically active subunit while METTL14 and WTAP play structural and localization roles, respectively [5]. Once the RNA is m^{6}A-modified, m^{6}A-binding proteins (readers) recognize and bind to the modified RNA. Well-known "readers" include YTHDC2, YTHDF1, YTHDF2 and YTHDF3 in the cytoplasmic compartment, as well as YTHDC1 in the nucleus. Removal of the m^{6}A modification is carried out by m^{6}A-demethylases (erasers) such as fat mass and obesity-associated protein (FTO) and AlkB homolog 5 (ALKBH5). These m^{6}A modification-associated proteins have been implicated in various diseases, including cancer [6] and autoimmune conditions [7]. Moreover, m^{6}A modifications have also been observed in viral genomes and RNAs, where they regulate viral replication cycles.

Although the roles of m^{6}A modification in viral life cycles remain unconfirmed, it has been reported to have regulatory effects in both DNA and RNA viruses. The m^{6}A modification has been extensively studied in the context of the human immunodeficiency virus (HIV), where it promotes viral RNA nuclear export and gene expression [8, 9]. Conversely, m^{6}A modification has antiviral effects in severe acute respiratory syndrome coronavirus 2 (SARS-CoV-2) and porcine epidemic diarrhea virus (PEDV) infections [10, 11]. In the case of Epstein–Barr virus (EBV), the "writer" protein METTL14 has been implicated in EBV-induced tumorigenesis [12]. Since m^{6}A appears to exert influence at many steps in virus life cycles, a comprehensive understanding of the impact of m^{6}A modification on viral infection cycles requires further investigation.

CONTACT Bobo Wing-Yee Mok bobomok@hku.hk Department of Microbiology, Li Ka Shing Faculty of Medicine, The University of Hong Kong, Pokfulam, Hong Kong Special Administrative Region, People's Republic of China; State Key Laboratory for Emerging Infectious Diseases, The University of Hong Kong, Pokfulam, Hong Kong Special Administrative Region, People's Republic of China; Honglin Chen hlchen@hku.hk Department of Microbiology, Li Ka Shing Faculty of Medicine, The University of Hong Kong, Pokfulam, Hong Kong Special Administrative Region, People's Republic of China; State Key Laboratory for Emerging Infectious Diseases, The University of Hong Kong, Pokfulam, Hong Kong Special Administrative Region, People's Republic of China; Centre for Virology, Vaccinology and Therapeutics Limited, The University of Hong Kong, Pokfulam, Hong Kong Special Administrative Region, People's Republic of China

Supplemental data for this article can be accessed online at https://doi.org/10.1080/22221751.2025.2572761.

Influenza A virus (IAV) was the first virus in which m^6A modifications were discovered on viral mRNAs [13]. Approximately 24 m^6A residues are distributed unevenly across different viral segments in IAV [13, 14]. Detailed mapping of m^6A residues in IAV was not unveiled for several decades, until Courtney et al., performed PA-m^6A-seq [15], a technique that pinpoints m^6A sites to within a range of approximately 23 nucleotides [16]. Their study also utilized METTL3 knockout cells and m^6A-deficient virus mutants to demonstrate the importance of m^6A modification in IAV replication, focusing in particular on how m^6A affects the expression of the HA gene of IAV. Subsequently, another study reported that the m^6A "reader" protein YTHDC1 regulated IAV replication by inhibiting NS mRNA splicing [17]. A m^6A site on the NS segment was then identified, based on the previous PA-m^6A-seq data [18]. A later study focusing on the host immune response found that m^6A modifications boost the innate response during IAV infection through the TBK1/METTL3 axis [19]. These findings suggested that m^6A modification played a critical role in the life cycle of IAV, although the underlying regulatory mechanisms remained to be understood.

The NS1 protein of IAV has been proposed to function in many steps of the virus life cycle, including splicing regulation, suppression of host immune responses and transportation of viral RNA [20]. The regulatory role of NS1 in the splicing of the NS segment of IAV has been a subject of debate since it was first observed in two studies in 1994. Fortes et al., reported that NS1 obstructed its own splicing process [21]. In contrast, Lu et al., suggested that while NS1 hindered pre-mRNA splicing, it did not affect its own mRNA splicing [22]. It is important to note that both studies utilized transfection methods due to the limited accessibility of the reverse genetics system at that time [23]. In 2007, Garaigorta et al., employed an RNP reconstitution system to serve as a substitute infection model [24]. Using this system, they found that NS1 inhibited the splicing and nuclear export of collinear NS transcripts. Subsequently, Robb et al., applied the same RNP reconstitution system and concluded that NS1 did not impact viral mRNA splicing [25]. In this paper, they observed a higher splicing ratio of NEP/NS1 at 24 h post-transfection in the absence of NS1, with a slight decrease in the ratio at 48 h post-transfection in the presence of NS1 [25]. This conflicting data made it difficult to determine which result was more convincing. Despite using the same methodology, Robb et al., could not explain their differing conclusions from Garaigorta et al.,'s study. A more recent study based on the H7N9 influenza strain reported that NS1 inhibits NS segment splicing through binding to the host splicing factor SF2 using replicon system [26]. Given the conflicting research in this area, no definitive conclusion has yet been established.

In this study, we investigate the roles of NS1 and m^6A in regulating IAV NS mRNA processing. Specifically, we generate a mutant virus that can transcribe NS mRNA but not translate it into functional NS1 protein, an ideal platform for studying the role of NS1 in its own mRNA splicing under infection conditions. By using this mutant, we have found that NS1 inhibits its own splicing through m^6A modification. The regulatory influence of m^6A is conserved within IAV subtypes and strains, with NS1 serving as the mediator for the addition of m^6A to NS mRNA. Consequently, our discovery sheds light on the mechanism by which m^6A regulates NS splicing in IAV, offering an alternative and broad-spectrum target for IAV therapy.

Materials and methods

Cell culture and transfection

Human embryonic kidney 293 T cells (HEK 293 T; ATCC:CRL-11268; RRID:CVCL_0063), human lung carcinoma A549 cells (A549; ATCC:CCL-185; RRID:CVCL_0023), normal African green monkey kidney epithelial cells (Vero; ATCC:CCL-81; RRID:CVCL_005) and chicken embryo fibroblasts (DF-1; ATCC:CRL-12203; RRID:CVCL_0387) were cultured in Dulbecco's Modified Eagle Medium (DMEM) with 10% Fetal Bovine Serum (FBS) (Life Technologies), 100 U/mL penicillin and 100 μg/mL streptomycin (Life Technologies), while Madin-Darby canine kidney cells (MDCK, ATCC:CCL-34; RRID:CVCL_0422) were cultured in Minimum Essential Medium (MEM) supplemented with the same concentrations of FBS and penicillin/ streptomycin. Cells were cultured at 37°C in a 5% CO_2 atmosphere. All cell lines used were routinely monitored for mycoplasma by PCR testing. Plasmids were transfected into cells using TransIT-LT1 Transfection Reagent (Mirus Bio) according to the manufacturer's protocol.

Viruses

Mutant viruses used in this study were generated using the backbone of the influenza virus strain A/WSN/1933 (H1N1) (WSN), creating a model for mechanistic exploration. Reverse genetics procedures were performed as previously described [23]. Other wild type influenza viruses used in this study include A/California/04/2009 (H1N1), A/Hong Kong/1-6-MA21-1/1968 (H3N2), A/Vietnam/1194/2004 (H5N1), and A/chicken/Guangdong/V/2008 (H9N2).

Plasmid construction and site-directed mutagenesis

Expression plasmids YTHDC1 (#85167) and METTL14 (#53740) were from Addgene. METTL3 was amplified by PCR using cDNA from A549 cells

and was constructed into the pcDNA3.1-FLAG vector. NS1 and NEP sequences from WSN were also cloned into pcDNA3.1-FLAG vector for expression. NS segment mutations were introduced into pHW2000 using exonuclease III, as previously described [27]. Primers used in this study are listed in Table S1.

Co-immunoprecipitation and western blotting

HEK 293 T cells were transfected with the indicated expression plasmids using polyethylenimine (PEI, Polysciences). The cells were then infected with viruses of interest at a multiplicity of infection (MOI) of 2 for 6 h. For co-immunoprecipitation, cells were harvested by incubating with lysis buffer (50 mM Tris-HCl pH 7.5, 150 mM NaCl, 1% Triton X-100, 1 mM EDTA, 10% Glycerol, 1 × Protease inhibitor cocktail (Roche) for 30 min on ice. Cell lysates were centrifuged to remove cell debris and incubated with mouse anti-NS1 (GeneTex) at 4°C overnight. Agarose A+G beads (Beyotime) were added to the lysates and incubated for 2 h at 4°C. Unbound proteins were washed away using lysis buffer, and the beads boiled in 2 × SDS loading buffer. The bound proteins were subjected to western blot analysis. For RNase A treatment, the cell lysates were incubated with 20 μL/mL RNase A/T1 Mix (Thermo Fisher Scientific) for 30 min on ice before immunoprecipitation.

For western blotting, cells were harvested through incubation with lysis buffer (50 mM Tris-HCl pH 7.5, 150 mM NaCl, 1% Triton X-100, 1 mM EDTA, 10% Glycerol, 1 × Protease inhibitor cocktail (Roche)) for 30 min on ice. Cell lysates were then centrifuged to remove cell debris. The lysates were mixed with SDS loading buffer (Beyotime) and boiled for 10 min. Gel electrophoresis was performed as previously described [28]. Electrophoresis was carried out at a constant voltage of 100 V until the target proteins reached the desired degree of separation. After electrophoresis, the proteins were transferred to a nitrocellulose membrane (Bio-Rad) and blocked with 3% skim milk in PBS for 30 min. Following two repeated 0.3% PBST washes, the membrane was incubated with primary antibody at 4°C overnight. After incubation, the membrane was incubated with secondary antibody (IRDye-680 or −800, LI-COR Biosciences) at room temperature for 60 min. Finally, the membrane was washed 5 times with PBST (5 min per wash) in preparation for scanning using the Azure Sapphire Biomolecular Imager.

Antibodies

Antibodies used in this study: anti-IAV NS1 (GeneTex, GTX125990), anti-IAV NEP (GeneTex, GTX125953), anti-NP (Laboratory-made [27]), anti-GAPDH (Abcam, ab8245), anti-SRSF3 (Abcam, ab198291), anti-β-Actin (Abcam, ab8226), anti-YTHDC1 (Abcam, ab259990), anti-METTL3 (Cell Signalling Technology, 86132), anti-METTL14 (Proteintech, 26158-1-AP), anti-FTO (Abcam, ab126605), anti-WTAP (Proteintech, 60188-1-Ig), anti-ALKBH5 (Proteintech, 16837-1-AP), anti-m^{6}A (Cell Signalling Technology, 56593), anti-mouse IgG (Proteintech, B900620), anti-rabbit IgG (Proteintech, 30000-0-AP).

RNA fluorescence in situ hybridization (FISH)

A549 cells were cultured on 8-chamber slides and infected at an MOI of 5 for the indicated number of hours. Subsequently, the cells were fixed for 15 min in 4% paraformaldehyde (PFA) and incubated in 75% ethanol at 4°C overnight. Cells were then permeabilized through treatment with 0.5% Triton X-100 for 10 min. For hybridization, the cells were incubated with RNA probes (Supplementary file 2) at 37°C for 6 h in a hybridization buffer (1 mL hybridization buffer: 100 μL formamide, 100 μL 20 × SSC, 200 μL 50% dextran sulfate, 600 μL H_2O). Following hybridization, the chamber slides were washed twice for 5 min each time using wash buffer containing 10% formamide and 10% SSC in H_2O. Cells were then labelled with secondary antibody at 37°C for 1 h. After incubation, the cells were washed with wash buffer three times, for 10 min each wash. The slides were mounted with mounting buffer containing DAPI (VECTASHIELD) in preparation for analysis under confocal microscopy.

RNA extraction and quantitative-real time RT–PCR

Cells were collected at the indicated time points after infection with viruses. Total RNA was isolated using an RNA isolation kit (Vazyme). Reverse transcription and quantitative real-time PCR (RT-qPCR) were carried out according to the manufacturer's protocol (Vazyme). Primers used for qPCR in this study are listed in Table S1.

RNA-immunoprecipitation qPCR (RIP-qPCR)

NS mRNAs associated with proteins were isolated as previously described [29]. Briefly, A549 cells were plated and allowed to reach 90-100% confluency before starting the experiment. Specific viruses at an MOI of 2 were used to infect cells for the indicated time periods. After infection, the cells were washed twice with PBS and subjected to UV crosslinking (150 mJ/cm^2). Next, cells were harvested and lysed in lysis buffer (50 mM Tris-HCl pH 7.5, 150 mM NaCl, 1% Triton X-100, 1 mM EDTA, 10% Glycerol, 1 × Protease inhibitor cocktail (Roche), RNase inhibitor

(Invitrogen)) for 30 min on ice. The lysates were then centrifuged at 16,000 g for 15 min at 4°C. Antibodies of interest were bound to agarose beads at 4°C for 1 h before their addition to lysates. Ten percent of each lysate was reserved as input sample, while the remaining lysate was incubated with antibody-bead complexes at 4°C overnight. After incubation, the beads were washed 5 times with RIP buffer (150 mM KCl, 25 mM Tris-HCl (pH 7.4), 5 mM EDTA, 0.5 mM DTT, 0.5% NP40) supplemented with RNase inhibitor. The beads were then treated with a Proteinase K solution (for each condition: 126 µL PBS, 15 µL 10% SDS, 9 µL 20 mg/mL Proteinase K) at 55°C for 30 min to release RNA and RNAs subsequently extracted using an RNA isolation kit (ZYMO RESEARCH). The RNA was then reverse transcribed and analyzed by qPCR. The interaction between RNA and protein was normalized to input.

For methylated RNA immunoprecipitation (MeRIP-qPCR), A549 cells were cultured until 90–100% confluency and infected with the specified viruses at an MOI of 2 for 6 h. Following infection, cells were washed twice with PBS and harvested without UV crosslinking. Cell lysis was performed using the same lysis buffer as described above, followed by centrifugation at 16,000 ×g for 15 min at 4 °C. The m^6A-specific antibody was bound to agarose beads at 4 °C for 1 h before incubation with the lysates. Ten percent of each lysate was reserved as input, and the remainder was incubated with the antibody-bead complexes overnight at 4 °C. Beads were then washed five times with RIP buffer containing RNase inhibitor. RNA was eluted and purified using an RNA isolation kit (ZYMO RESEARCH), followed by reverse transcription and qPCR analysis. Enrichment of methylated RNA was normalized to the input samples.

Nanopore-based direct RNA sequencing (DRS-sequencing)

For nanopore sequencing of IAV-infected A549 cells, total RNA was extracted using the E.Z.N.A.®-Total RNA Kit I (Omega, R6834) from samples collected at 3 and 9 h.p.i.. Following RNA quality assessment, poly(A) mRNA was isolated from 20 µg of total RNA per sample using the poly(A) selection kit (NEB, E7490S) according to the manufacturer's instructions. The enriched mRNA was then used to construct sequencing libraries in accordance with the Oxford Nanopore DRS guidelines (SQK-RNA004). Library preparation involved ligating the Nanopore RT adapter to the mRNA using T4 DNA ligase (NEB M0202M). The adapter-ligated mRNA was reverse transcribed to generate cDNA, which was subsequently purified using Agencourt RNAClean XP beads (Beckman Coulter). An RNA sequencing adapter was then ligated to the cDNA, followed by a second purification step with RNA-Clean XP beads to remove excess adapters and contaminants. The final library was loaded onto a FLO-PRO004RA flow cell and sequenced on a PromethION platform (Oxford Nanopore Technologies, UK) for 48–72 h. Sequencing was performed in three independent biological replicates to enable robustness and enable real-time single-molecule analysis. Raw data in fast5 format were base-called using Dorado and subsequently converted to fastq format for downstream processing.

RNAi and lentiviral transduction

Knockdown of RNA in A549 cells was performed using siRNAs purchased from Integrated DNA Technologies (IDT, hs.Ri.SRSF3.13.2 and hs.Ri.SRSF3.13.3). Transfection of siRNAs was carried out using Lipofectamine RNAiMAX Transfection Reagent (Invitrogen) according to the manufacturer's instructions. After two days of transfection, cells were infected with the indicated viruses without reseeding cells.

For knockout, lentiviruses were added to A549 cells along with 10 µg/mL polybrene (Invitrogen). The medium was replaced after 8 h. Cells were then selected by incubating with puromycin (1 µg/mL for A549 cell line) for 72 h and knockout confirmed by sequencing and western blot analysis. To knockout YTHDC1, the gRNA sequence: 5′-tgattatgacactc-gaagtg-3′ was selected.

Plaque assay and viral growth kinetics

MDCK cells were cultured on 6-well plates until they reached 100% confluency. Viruses were diluted in a 10-fold serial manner using MEM medium. Cells were infected with 100 µL of the prepared serially diluted viruses. After an hour absorption period the supernatant was removed and the cells overlayed with 2 mL of 1% MEM agarose containing 1 µg/mL TPCK-treated trypsin. The plates were incubated at 37°C for 2 days to allow viral replication. Agarose overlays were then removed, and the cells fixed with 10% formaldehyde. To visualize plaques, the cells were stained using 1% crystal violet.

For growth kinetics analysis, A549 cells were grown to 100% confluency in 48-well plates. The cells were infected with the indicated viruses at an MOI of 0.01. After 1 h of absorption, the supernatant was removed, and the cells were washed twice with PBS. The cells were then cultured in MEM medium containing 1 µg/mL TPCK-treated trypsin. At the specified time points, culture supernatants were collected and titrated by plaque assay to determine the viral concentration.

Pull down assay and mass spectrometry

A549 cells were transfected with a vector containing NS mRNA for 48 h. After transfection, the cells were washed twice with PBS and subjected to UV cross-linking (150 mJ/cm^2). Following irradiation, cells were lysed on ice for 30 min in lysis buffer (50 mM Tris-HCl (pH 7.5), 150 mM NaCl, 1% Triton X-100, 1 mM EDTA, 1 × Protease inhibitor cocktail (Roche), RNase inhibitor (Invitrogen)). Concurrently, biotinylated probes targeting NS mRNA (probe1: 5′ cctgaaagcttgacacagtgtttggatc 3′-biotin; probe2: 5′ atgcaggtacagaggccatggtcattttga 3′-biotin) were pre-incubated with streptavidin-coated magnetic beads to allow probe-bead conjugation. The cell lysates were then mixed with the probe-bead complexes and incubated overnight at 4°C with gentle rotation. The beads were then washed extensively to remove non-specifically bound RNAs. Finally, the bound RNAs were eluted and purified for subsequent liquid chromatography-tandem mass spectrometry (LC-MS/MS) analysis.

Statistical analysis

Student's t-tests was used in this study. Symbols used to represent P values are: * $P < 0.05$, ** $P < 0.01$, *** $P < 0.001$ and **** $P < 0.0001$. Error bars indicate mean ± SD for triplicate (or greater) biological experiments (n≥3). All statistical analyses and plotting were performed using GraphPad Prism 9.

Data availability

The DRS sequencing dataset generated in this study has been deposited in the GEO database under accession number GSE308596.

Results

NS1 negatively regulates NS mRNA splicing

Research groups utilizing transfection systems have published conflicting conclusions regarding the role of NS1 in regulating its own mRNA splicing. To address this question in the context of viral infection, we generated a mutant virus, WSN/Ans1 (Figure 1A), which transcribes NS mRNA but is unable to translate this into functional NS1 protein due to the insertion of two stop codons in the open reading frame of NS mRNA [30]. We infected A549 and Vero cells with this mutant virus to examine its growth kinetics. Our findings demonstrated that the absence of NS1 protein significantly inhibited viral replication in Vero cells (Figure 1B). However, no WSN/Ans1 plaques formed in A549 cells at all (Figure S1A). Given that Vero cells are IFN-deficient [31], the profound replication deficiency in IFN-competent A549 cells suggests that the WSN/Ans1 mutant undergoes single-round infection in this type of cellular environment (A549 cells).

To further confirm the regulatory role of NS1 in its own splicing, we infected A549 cells with WSN/WT and WSN/Ans1 and evaluated the levels of NS1 and NEP mRNA using RT-qPCR. Our results showed that the absence of NS1 increased the NEP/NS1 ratio, due to elevated splicing efficacy (Figure 1C). Furthermore, we examined the expression levels of NS1 and NEP proteins during WSN/WT and WSN/Ans1 infections. As expected, WSN/Ans1 did not express NS1; however, NEP was also undetectable by western blotting (Figure S1B). To exclude the potential effect of the undetectable of NEP on NS mRNA splicing, we performed two experiments: (1) Since NEP has been found to be crucial for export of viral RNA from the nucleus to the cytoplasm [32, 33], we investigated the localization of viral RNA (vRNA) in WSN/Ans1-infected cells, finding that vRNAs from all genome segments are still exported to the cytoplasm, albeit less efficiently than vRNAs in wild-type (WT) virus infections (Figure S1C). This reduced vRNA export correlates with the observed attenuation in replication shown in Figure 1B. (2) Exogenous NEP protein supplementation during WSN/Ans1 infection did not affect splicing efficiency (Figure S1D), indicating that the altered splicing is unrelated to NEP deficiency. Collectively, these data indicate that NS1 itself negatively regulates its own mRNA splicing.

NS1 enhances m^{6}A addition on NS mRNA

It is well-established that RNA viruses often hijack host factors to facilitate their replication. To investigate host factors involved in NS mRNA splicing, we conducted RNA pull-down followed by LC-MS/MS (Figure 2A). Among the top candidates pulled down by NS mRNA, we detected the m^{6}A reader YTHDC1, which has been reported to be involved in splicing [17, 34] (Figure 2B and Supplementary File 3). This finding prompted us to investigate whether methylation plays a role in regulation of NS mRNA splicing. Examining the role of YTHDC1 in viral replication, we found that WSN/WT virus exhibited attenuated replication in YTHDC1 knockout (KO) cells compared to control cells (Figure 2C).

As YTHDC1 recognizes m^{6}A modifications, we hypothesized that NS mRNA might carry this marker. We validated this by performing an RNA-immunoprecipitation assay. As shown in Figure 2D, we observed that NS mRNAs were indeed m^{6}A modified, as evidenced by their enrichment compared to the m^{6}A-modified positive control (SON) and the negative control (HPRT1). Given NS1′s suppression of its own splicing, we investigated whether this function is related to m^{6}A modification. Specifically, the absence of NS1 protein resulted

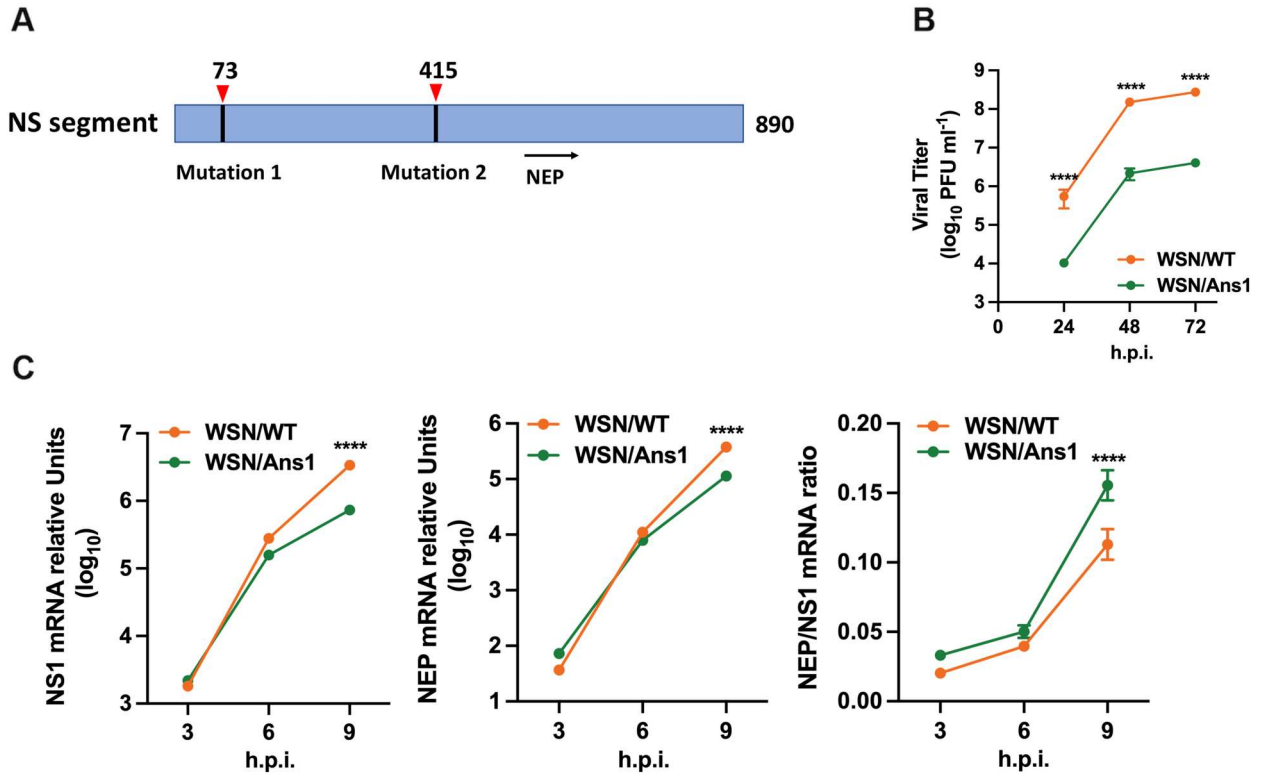

Figure 1. Negative regulation of NS mRNA splicing by NS1 (**A**) Schematic illustration of NS1 mutant construction (WSN/Ans1). Two stop codons have been introduced into the NS segment, thereby enabling transcription but preventing translation into a functional NS1 protein. (**B**) Growth kinetics of WSN/WT and WSN/Ans1. Vero cells were infected with WSN/WT and WSN/Ans1 viruses at an MOI of 0.01. Supernatants were harvested at the indicated time points and viruses titrated by plaque assay. Error bars represent the mean ± SD (n = 3). Statistical significance was assessed using Student's t-test: ****P<0.0001; h.p.i., hours post-infection. (**C**) mRNA levels of NS genes in WSN/WT and WSN/Ans1 infections. Total RNA from A549 cells infected with the WSN/WT and WSN/Ans1 viruses at an MOI of 2 was isolated at the indicated time points. Quantification of NS1 and NEP mRNAs was performed by RT–qPCR. Error bars represent the mean ± SD (n = 3). Statistical significance was determined using Student's t-test: ****P<0.0001; h.p.i., hours post-infection.

in a slightly increased m^{6}A modification level in viral polymerase and NP genes, while other viral genes exhibited a decrease in m^{6}A modification (Figure 2E). The most pronounced change was observed in NS mRNA, suggesting that NS1 primarily regulates m^{6}A modification on its own mRNA.

To verify this result, we examined m^{6}A modification levels under transfection conditions. Our results showed that NS1 promotes m^{6}A addition on both its own and host mRNA, with a more significant effect on the former (Figure 2F). Furthermore, a rescue and overexpression experiment demonstrated that progressively increasing doses of NS1 initially lead to increased m^{6}A modification levels. However, beyond a certain point, further elevation of NS1 resulted in a decline in m^{6}A levels (Figure 2G-H), indicating that NS1 may regulate m^{6}A addition onto its own mRNA via a negative feedback loop. We next examined whether NS1-mediated feedback operates through inhibition of the m^{6}A writers or recruitment of erasers. Co-IP analysis identified METTL3 (writer) and ALKBH5 (eraser) as the primary components of the m^{6}A machinery interacting with NS1 within their respective groups (Figure S2A). Subsequent RIP assays demonstrated that increasing NS1 concentrations led to a significant reduction in METTL3 binding to NS mRNA, consistent with the observed decrease in m^{6}A methylation (Figure S2B). In contrast, the interaction between ALKBH5 and NS mRNA exhibited a different pattern, with a slight rebound at the highest NS1 level (Figure S2C), suggesting a minor contribution from eraser recruitment.

Similar to the NS segment, WSN/Ans1-infected cells exhibited an elevated splicing ratio for the M segment compared to WSN/WT-infected cells (Figure 2I), aligning with previous findings regarding the influence of viral NS1 on the ratio of M1 to M2 protein production [35]. These results imply that NS1 protein influences the splicing process beyond that of its own mRNA, indicating a broader regulatory role.

To further elucidate how NS1 regulates the addition of m^{6}A modifications, we analyzed the expression levels and subcellular distribution of m^{6}A-associated host proteins in cells infected with WSN/WT and WSN/Ans1. No significant alterations were observed in the expression levels (Figure S2D) or subcellular localization (Figure S2E) of these proteins between the two conditions. Figure S2F shows that NS1

interacts with m^{6}A writers through m^{6}A modification. Collectively, these findings suggest that NS1 influences viral mRNA splicing by modulating m^{6}A addition through its interactions with m^{6}A writers.

The A385 residue of the NS segment is m^{6}A-modified

To map m^{6}A modification sites on NS mRNA, we employed a modified MeRIP-RT-qPCR approach. This method relies on the principle that m^{6}A modification impedes single-base elongation activity of DNA polymerases and decreases nick ligation efficiency. As illustrated in Figure 3A, primers were designed targeting NS mRNA for two rounds of m^{6}A enrichment. The two-stage enrichment process revealed extension blockage in the ED region and failure of Segment_3 amplification (Figure 3B), thereby localizing the m^{6}A modifications to Segment_3. Given the presence of a m^{6}A-typical DRACH motif (where D = A/G/T,

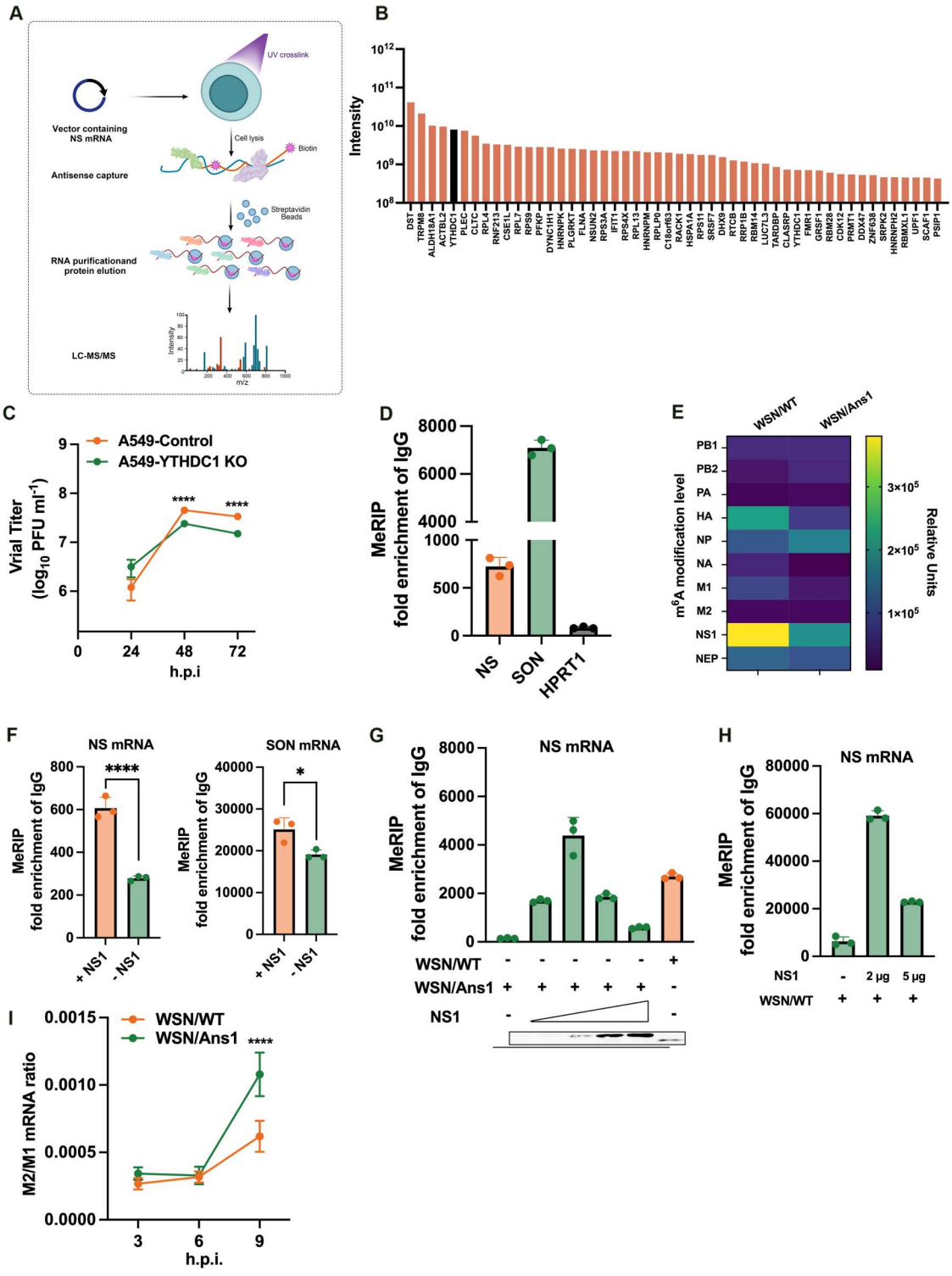

R = A/G, H = A/C/T) within Segment_3, these results suggest that there was an m^{6}A modification site at A385 on the NS segment (Figure 3C). We then employed nanopore-based direct RNA sequencing (DRS) to validate these data. This technology enables direct sequencing of native RNA or DNA, allowing for precise identification of modification sites on the viral genome. The m^{6}A modification map of the IAV genome is presented in Figure 3D. The distribution of m^{6}A modifications exhibited remarkable similarity between the early and later stages of WSN/WT infection (Figure S3A), further supporting the validity of our findings. Additionally, we utilized SRAMP (sequence-based RNA adenosine methylation site predictor) for m^{6}A site prediction, marking the sites with highest confidence in red (Figure S3B). Notably, all data from RIP, DRS, and SRAMP consistently identified A385 as an m^{6}A-modified site on NS mRNA.

To functionally characterize A385, we generated a WSN/A385C mutant virus. As expected, the A385C mutation significantly affected m^{6}A levels on NS mRNA in WSN/A385C mutant infections compared to wild type virus infections (Figure 3E). Since A385C is a nonsynonymous mutation, we wanted to determine whether changes in the NS1 protein could influence NS mRNA modification levels. Therefore, we overexpressed NS1 proteins from both wild type and A385C viruses in WSN/Ans1-infected cells and assessed m^{6}A levels. The results showed that both WT NS1 and A385C NS1 significantly enhanced the m^{6}A level of NS mRNA in WSN/Ans1 virus infections, indicating that the amino acid alteration had no significant impact on m^{6}A modification. Thus, the observed decline in m^{6}A levels in the WSN/A385C mutant is attributable solely to the nucleotide change, rather than to alterations in the amino acid sequence (Figure 3F). Phenotypic analysis revealed that A385C mutation impaired viral replication in Vero cells (Figure 3G) and enhanced NS mRNA splicing in A549 cells (Figure 3H). These findings conclusively demonstrated that m^{6}A modification at position A385 is important for IAV replication and required for regulation of NS segment splicing.

Evolutionary preservation of m^{6}A-mediated splicing regulation in IAV

To investigate evolutionary changes at the m^{6}A modification site, we analyzed 79,404 human and non-human IAV sequences retrieved from the Influenza Research Database (Supplementary File 4). The A385 residue exhibited remarkable conservation (Figure 4A), indicating its likely critical functional significance. Next, we investigated m^{6}A modification at the A385 site in NS mRNA from four evolutionary diverse IAV strains representing different subfamilies (Figure S4A). These included three outbreak isolates - A/California/04/2009 (CA4), A/Hong Kong/1-6-MA21-1/1968 (HK68), and A/Vietnam/1194/2004 (1194) - as well as one avian-origin strain, A/chicken/Guangdong/V/2008 (GDV). To confirm the presence of m^{6}A sites within these strains, we employed the MeRIP-RT-qPCR approach using primers spanning the entire NS segment. The results demonstrated that at least one m^{6}A modification site is present in the NS mRNA of each strain (Figure S4 B–E). For clarity, the regions of interest within these segments from the four strains are highlighted, with

Figure 2. NS1 enhances m^{6}A addition to NS mRNA. (**A**) Experimental procedure for the identification of host factors interacting with NS mRNA using mass spectrometry. (**B**) The MS/MS spectrum of the identified YTHDC1 peptide immunoprecipitated by NS mRNA. (**C**) Growth kinetics of WSN/WT in the absence of YTHDC1. Infection of either A549 or A549-YTHDC1 knockout cells with WSN/WT at an MOI of 0.01. Supernatants were harvested at the indicated time points and viruses titrated by plaque assay. Error bars represent the mean ± SD (n = 3). Statistical significance was assessed using Student's t-test: ****P<0.0001; h.p.i., hours post-infection. (**D**) m^{6}A modification level of NS mRNA in WSN/WT infection. SON and HPRT1 serve as positive and negative controls, respectively. A549 cells were infected with WSN/WT for 6 h. Equal amounts of RNA subjected to immunoprecipitation using either a control IgG antibody or an anti-m^{6}A antibody, followed by extraction and RT-qPCR analysis of the immunoprecipitated RNA. Error bars represent the mean ± SD (n = 3). (**E**) m^{6}A modification levels of IAV genome segments. A549 cells were infected with either WSN/WT or WSN/Ans1 for 6 h. The cells were then lysed, and equal amounts of RNA subjected to immunoprecipitation using either a control IgG antibody or an anti-m^{6}A antibody. Immunoprecipitated RNA was extracted and subjected to RT-qPCR using specific primers for viral genes. Data is presented as the mean from three independent experiments. (**F**) m^{6}A modification levels of (**Left panel**) viral and (**Right panel**) host mRNAs. HEK 293 T cells were transfected with either NS1 overexpression vector or empty vector, together with Ans1 vector for NS mRNA transcription. After 48 h, cells were lysed, and equal amounts of RNA from each experimental condition subjected to immunoprecipitation using either a control IgG antibody or an anti-m^{6}A antibody. Immunoprecipitated RNA was extracted and subjected to RT-qPCR using NS and SON gene-specific primers. Error bars represent the mean ± SD (n = 3). Statistical significance was determined using Student's t-test: *P<0.05 and ****P<0.0001. (**G**) Impact of NS1 overexpression on m^{6}A levels in WSN/Ans1 infection. HEK 293 T cells were transfected with increasing doses of an NS1 overexpression vector. After 48 h, the cells were infected with WSN/Ans1 or (**H**) WSN/WT for 6 h. Equal amounts of RNA were subjected to immunoprecipitation using either a control IgG antibody or an anti-m^{6}A antibody, followed by extraction and RT-qPCR analysis of the immunoprecipitated RNA. Error bars represent the mean ± SD (n = 3). (**I**) M segment splicing ratio in WSN/WT and WSN/Ans1 infections. Total RNA from A549 cells infected with WSN/WT and WSN/Ans1 viruses at an MOI of 2 was isolated at the indicated time points. Quantification of M1 and M2 mRNAs was performed by RT–qPCR. Error bars represent the mean ± SD (n = 3). Statistical significance was determined using Student's t-test: ****P<0.0001; h.p.i., hours post-infection.

segments showing lower fold enrichment being more lightly shaded (Figure 4B). We found that the A385 site was located at those identified region across all strains tested.

To further confirm the functional significance of the conserved A385 site in NS mRNA, mutant viruses carrying the A385C mutation (corresponding to position A370C in strain 1194) were generated for all four strains (Figure S4F). As shown in Figure 4C, all mutants across the four strains exhibited significantly reduced m^{6}A modification levels compared to their wild-type counterparts, confirming the essential role of A385 in m^{6}A modification.

Building on our previous demonstration of the role of m^{6}A modification at the A385 site in NS mRNA in regulating its own splicing in WSN, we aimed to investigate whether this regulatory function is conserved across different IAV strains. We confirmed that the

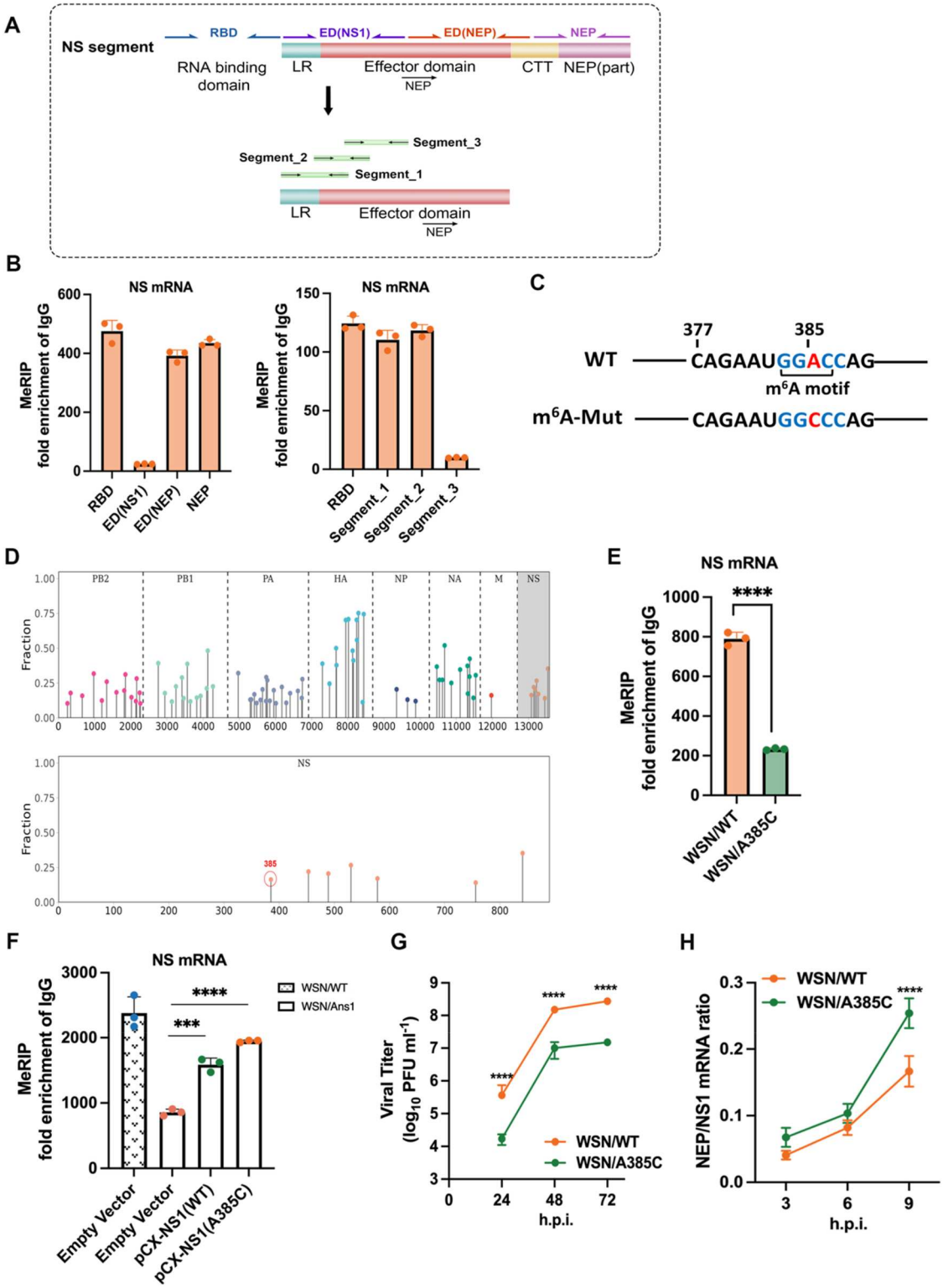

NEP/NS1 mRNA splicing ratio was increased for A385C mutant (m^6A-deficient) viruses compared to wild-type strains during human IAV strain infections (HK68, CA4, and 1194) in A549 cells, as well as infections involving the avian-origin GDV strain in both mammalian (A549) and avian (DF-1) cells (Figure 4D). Notably, the difference between GDV/WT and GDV/A385C was much less pronounced in infected A549 cells than in infected DF-1 cells, suggesting that while A385 functions as a conserved m^6A modification site influencing NS segment splicing, its impact may vary between human- and avian-origin IAV strains, likely through similar mechanisms with some degree of species-specific modulation.

m^6A-mediated control of NS mRNA splicing via competitive binding of YTHDC1 and SRSF3 to NS mRNA

The observed association between m^6A modification and NS mRNA splicing, along with the identification of NS mRNA interaction with YTHDC1 through mass spectrometry, suggests that YTHDC1 plays a crucial role in the splicing of NS mRNA. To address this, we knocked out YTHDC1 in A549 cells, observing a notable increase in the splicing ratio of NS mRNA in its absence (Figure 5A). Previous reports have evidenced collaboration between YTHDC1 and SRSF3 in the regulation of mRNA splicing [34]. To study the involvement of SRSF3 in NS mRNA splicing, we knocked down SRSF3 protein in A549 cells, followed by infection with WSN/WT. The results revealed that knockdown of SRSF3 led to a reduced NEP/NS1 splicing ratio, indicating a facilitative role for SRSF3 in NS mRNA splicing (Figure 5B). These findings collectively suggest that YTHDC1 and SRSF3 play different roles in NS mRNA splicing.

To further investigate the interplay between YTHDC1 and SRSF3, we conducted RNA immunoprecipitation assays. As shown in Figure 5C, NS mRNA of WSN/WT displayed increased affinity for SRSF3 when YTHDC1 was absent, compared to WSN/WT infections in control A549 cells. Similarly, SRSF3 exhibited stronger binding to NS mRNA from WSN/A385C than to that from WSN/WT. This is presumably due to the absence of YTHDC1 binding, as NS mRNA from WSN/A385C does not associate with YTHDC1. These findings suggest that SRSF3 binds more avidly to NS mRNA when m^6A modification or YTHDC1 is absent, indicating a potential competitive interaction between YTHDC1 and SRSF3. To validate this hypothesis, we conducted additional RNA immunoprecipitation assays. Our results demonstrated that overexpression of increasing levels of YTHDC1 in WSN/WT-infected cells led to a

Figure 3. A385 site on NS mRNA is m^6A modified and required for regulation of NS mRNA splicing. (**A**) This figure illustrates the full-length structure of the NS segment, represented by the entire bar, with distinct colours indicating its various domains. To identify the m^6A modification site, a two-round selection strategy was employed. In the first round, four pairs of primers spanning the entire NS segment were used for qPCR analysis. In the second round, three additional pairs of primers targeting the ED(NS1) domain were utilized to precisely locate m^6A modification sites. LR: linker region, CTT: C terminal tail. (**B**) Localization of m^6A-modified sites on NS mRNA using a modified MeRIP-RT-qPCR approach. A549 cells were infected with the WSN/WT virus at an MOI of 2 for 6 h. Two rounds of MeRIP-RT-qPCR were performed to identify m^6A-modified sites. Equal amounts of RNA were immunoprecipitated using either a control IgG antibody or an anti-m^6A antibody, followed by RT-qPCR analysis. (**Left panel**) The first round of MeRIP-RT-qPCR utilized primers spanning the entire length of the NS segment. (**Right panel**) The second round of MeRIP-RT-qPCR employed primers targeting the ED(NS1) region. All results were normalized to the IgG control group, with the input RNA used as the reference. Error bars represent the mean ± SD (n = 3). (**C**) Conserved m^6A motif identified by MeRIP-RT-qPCR. A 5′-DRACH-3′ sequence (where A represents the methylatable adenosine, D denotes A, G, or U), (R signifies A or G, and H stands for A, C, or U) was identified. To reduce the m^6A modification level, a mutant virus was engineered by substituting the central A with C (A385C), resulting in a deficiency in m^6A methylation. (**D**) Nanopore-based direct RNA sequencing (DRS) analysis of poly(A)-selected mRNAs extracted from IAV-infected A549 cells at 9 h post-infection. The top panel depicts m^6A modification sites across the IAV viral transcripts, with each dot representing an individual m^6A site. The bottom panel provides a magnified view of m^6A modifications on the NS segment. The X-axis indicates the transcript length, while the Y-axis shows the proportion of m^6A-modified reads relative to the total viral transcript reads (m^6A-modified reads divided by total reads). (**E**) m^6A modification level of NS mRNA in WSN/WT and WSN/A385C infections. A549 cells were infected with either WSN/WT or WSN/A385C for 6 h. The cells were then lysed, and equal amounts of RNA subjected to immunoprecipitation using either a control IgG antibody or an anti-m^6A antibody. Immunoprecipitated RNA was extracted and subjected to RT-qPCR (amend as appropriate). Error bars represent the mean ± SD (n = 3). Statistical significance was assessed using Student's t-test: ****P<0.0001. (**F**) Effect of the nonsynonymous mutation A385C on m^6A modification levels. HEK 293 T cells transfected with either empty vector, or vectors containing NS1(WT) or NS1(A385C) for overexpression. At forty-eight hours post-transfection, cells were infected with either WSN/WT or WSN/Ans1 at an MOI of 2 for 6 h and subsequently subjected to MeRIP-RT-qPCR analysis. Error bars represent the mean ± SD (n = 3). Statistical significance was assessed using Student's t-test: ***P<0.001 and ****P<0.0001. (**G**) Growth kinetics of WSN/WT and WSN/A385C in Vero cells. Supernatants were harvested at the indicated time points, and viral titres determined by plaque assay. Error bars represent the mean ± SD (n = 3). Statistical significance was assessed using Student's t-test: ****P<0.0001; h.p.i., hours post-infection. (**H**) Splicing ratios of the NS segment in WSN/WT and WSN/A385C infections. Total RNA was isolated from A549 cells infected with WSN/WT and WSN/A385C at an MOI of 2 at the indicated time points. NS1 and NEP mRNAs were quantified by RT–qPCR. Error bars represent the mean ± SD (n = 3). Statistical significance was determined using Student's t-test: ****P<0.0001; h.p.i., hours post-infection.

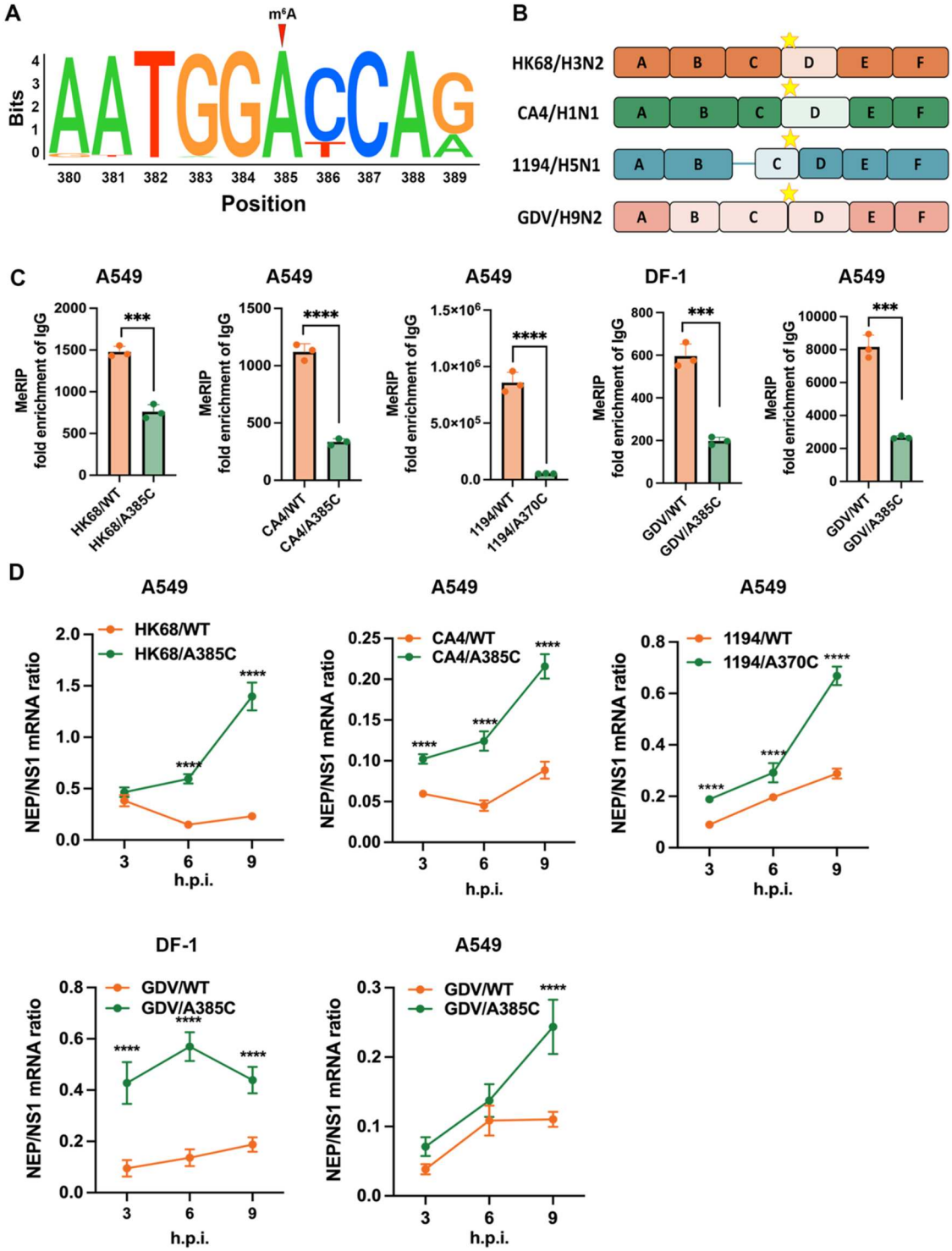

Figure 4. Evolutionary preservation of m^{6}A-mediated splicing regulation in IAV. (**A**) Conservation analysis of A385 in NS mRNA. Complete NS1 nucleotide sequences from all IAV strains isolated from both human and avian sources were retrieved from the NCBI Influenza A Virus Resource Database. Sequences were aligned, and a 10-base-pair segment spanning the 385-nucleotide region was extracted. Motif analysis results are visualized, with logos representing the relative frequency of nucleotides at positions −5 to +4 surrounding the central A residue. The motif analysis was performed using MEGA 10 and omictools from GENE DENOVO. (**B**) Primer regions highlighted on NS segments of various strains. Each colour corresponds to a different strain, with lighter shaded primer regions indicating potential m^{6}A modification sites identified by MeRIP-RT-qPCR (Figure S4B-E). A star on each segment marks the location of A385. (**C**) m^{6}A modification levels of NS mRNA in wild-type and A385 mutant viruses. m^{6}A levels were measured by MeRIP-RT-qPCR in A549 or DF-1 cells infected with the indicated viruses at an MOI of 2 for 6 h. Error bars represent the mean ± SD (n = 3). Statistical significance was determined using Student's t-test: ***P<0.001 and ****P<0.0001. (**D**) Splicing ratios for the NS segment in wild-type and m^{6}A-deficient versions of HK68, CA4, 1194 and GDV. Total RNA was isolated from A549 or DF-1 cells infected with wild-type and A385C mutant versions of different virus strains at an MOI of 2 at the indicated time points. Quantification of NS1 and NEP mRNAs was performed by RT–qPCR. Error bars represent the mean ± SD (n = 3). Statistical significance was determined using Student's t-test: ****P<0.0001; h.p.i., hours post-infection.

significant dose-dependent reduction in binding between SRSF3 and NS mRNA, suggesting that YTHDC1 does indeed interfere with the SRSF3-NS mRNA interaction (Figure 5D). Given that YTHDC1 appears to compete with SRSF3 for binding to NS RNA, we next examined whether SRSF3 binds to NS mRNA in close proximity to the A385 m^{6}A site.

To map the binding site of SRSF3 on NS mRNA, we conducted a modified RNA immunoprecipitation assay, utilizing the same strategy and primers as previously described [36, 37]. Briefly, after immunoprecipitation with an SRSF3-specific antibody to capture protein-RNA complexes, the samples were treated with Proteinase K to digest proteins while leaving residual amino acids at the binding sites. These remnants physically hinder DNA polymerase elongation during subsequent reverse transcription-quantitative PCR, leading to elevated Ct values. Our results

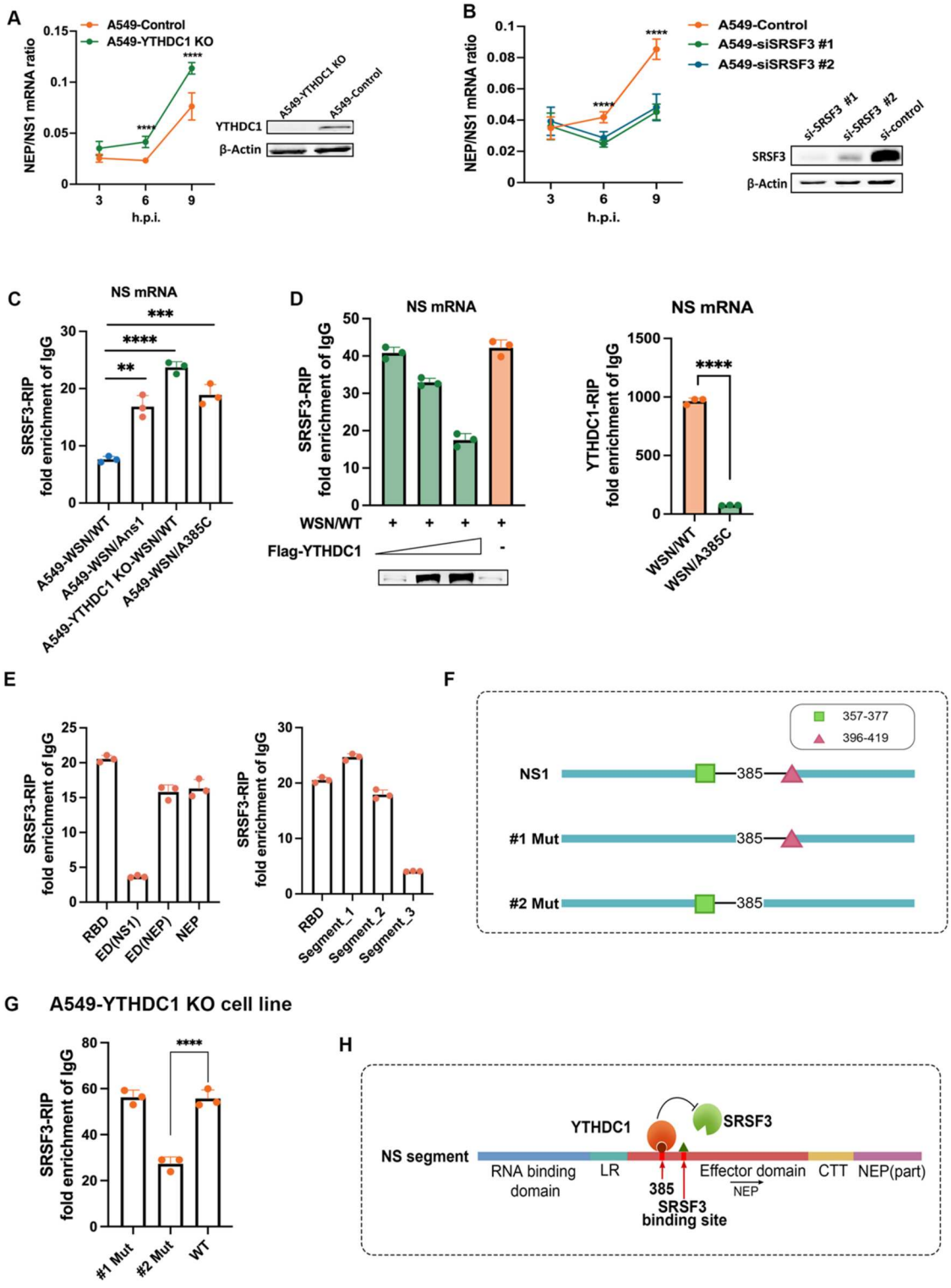

revealed that SRSF3 binds to Segment_3 within ED(NS1) (see Figure 3), which encompasses the m^{6}A binding region (A385) of NS mRNA (Figure 5E).

To further refine the binding site of SRSF3 on NS mRNA, we generated two NS mRNA mutants (#1 Mut and #2 Mut), each containing an ~20 bp sequence deletion from Segment_ 3 adjacent to position 385 (Figure 5F). Given the competition between YTHDC1 and SRSF3 for binding to NS mRNA, and the natural binding affinity between NS mRNA (WT) and YTHDC1, we performed the modified SRSF3-RIP-RT-qPCR experiment in YTHDC1 knockout cells. Our findings demonstrated that SRSF3 preferentially binds to #2 Mut, indicating that the binding site is located within the 396-419 bp region of NS mRNA (Figure 5G-H). These findings indicate that SRSF3 and YTHDC1 do not directly compete for the same m^{6}A marker on NS mRNA. Rather, it appears that m^{6}A modification at position 385 specifically recruits the reader protein YTHDC1, which presumably creates a steric barrier that prevents SRSF3 from accessing its binding site on the adjacent section of NS mRNA. This interference consequently diminishes the splicing activity of NS mRNA (Figure 5H).

Discussion

The NS1/NEP expression is critical for influenza A virus replication and is associated with the mechanisms underlying cross-species transmission of avian influenza A virus [26]. Since the NS1 protein is among the earliest expressed viral proteins, it is important to characterize its regulatory role in the processing of its own mRNA. The regulatory role of NS1 in its own mRNA processing remains limited and controversial in current understanding. In this study, our findings highlight the significance of NS1 expression and m^{6}A modification in NS mRNA splicing. Specifically, our study reveals that (1) NS1 inhibits its own mRNA splicing (Figure 1), (2) NS1 regulates m^{6}A addition onto its own mRNA through a negative feedback mechanism (Figure 2), (3) the regulatory role of m^{6}A modification (A385) in NS mRNA splicing is conserved across different strains (Figures 3–4), and that (4) NS mRNA is m^{6}A-modified and m^{6}A modification regulates NS mRNA splicing via the involvement of YTHDC1, which inhibits the binding of SRSF3 to NS mRNA, thus impeding splicing (Figure 5). Collectively, our study provides compelling evidence and informs a working model elucidating how NS1 regulates its own mRNA splicing via m^{6}A modification, as depicted in Figure 6.

Studying the viral life cycle under infection conditions is more persuasive than using the plasmid transfection systems. Using WSN/Ans1 mutant virus enabled us to discover that NS1 inhibits its own collinear mRNA splicing. Our study also revealed that NS1 plays a role in regulating m^{6}A addition to NS mRNA, indicating a negative feedback loop. This regulatory function of NS1 should not be viewed as solely positive or negative, as unidirectional regulation in either

Figure 5. YTHDC1 disrupts the interaction between SRSF3 and NS mRNA. (**A**) NS segment splicing ratio in A549-YTHDC1 knockout cells. A549 or A549-YTHDC1 knockout cells were infected with WSN/WT at an MOI of 2. Total RNA was extracted at the indicated time points. (**Left panel**) Levels of NS1 and NEP mRNAs were measured by RT–qPCR. Error bars represent the mean ± SD (n = 3). Statistical significance was determined using Student's t-test: ****P<0.0001; h.p.i., hours post-infection. (**Right panel**) Efficiency of YTHDC1 knockout was validated by western blot. (**B**) NS segment splicing ratios in A549-SRSF3 knockdown cells: A549 or A549-siSRSF3 knockdown cells were infected with WSN/WT at an MOI of 2. Total RNA was extracted at specific time points. (**Left panel**) Levels of NS1 and NEP mRNAs, measured by RT–qPCR. Error bars represent the mean ± SD (n = 3). Statistical significance was determined using Student's t-test: ****P<0.0001; h.p.i., hours post-infection. (**Right panel**) Efficiency of SRSF3 knockdown was validated by western blot. (**C**) Effect of YTHDC1 and m^{6}A modification on binding of SRSF3 to NS mRNA. A549 and A549-YTHDC1 knockout cells were infected with either wild-type or mutant WSN viruses at an MOI of 2. At six hours post-infection, cells were lysed, and equal amounts of RNA were immunoprecipitated using either a control IgG antibody or an anti-SRSF3 antibody. The immunoprecipitated RNA was extracted and analyzed by RT-qPCR. Error bars represent the mean ± SD (n = 3). Statistical significance was determined using Student's t-test: **P<0.01, ***P<0.001 and ****P<0.0001. (**D**) (**Left panel**) Influence of YTHDC1 overexpression on SRSF3-NS mRNA interaction. HEK 293 T cells were transfected with increasing doses of YTHDC1 overexpression vector. At 48 h, cells were infected with WSN/WT at an MOI of 2 for 6 h. Equal amounts of RNA were immunoprecipitated with control IgG or anti-SRSF3 antibodies, then extracted and analyzed by RT-qPCR analysis. (**Right panel**) YTHDC1 binding to NS mRNA in cells infected with WSN/WT and WSN/A385C viruses. A549 cells were infected with each virus for 6 h, followed by YTHDC1-RIP to assess binding levels. Error bars represent the mean ± SD (n = 3). (**E**) Identification of SRSF3 binding sites on NS mRNA using modified SRSF3-RIP-qPCR (as described in Figure 3A and B). A549 cells were infected with WSN/WT at an MOI of 2 for 6 h. Equal amounts of RNA were immunoprecipitated using either control IgG or anti-SRSF3 antibodies, followed by extraction and RT-qPCR analysis. **(Left panel)** Results from the first round of SRSF3-RIP with primers spanning the entire NS segment. **(Right panel)** Results from the second round of SRSF3-RIP using primers targeting the ED region of NS1. All data were normalized to the IgG control with the corresponding input RNA. Error bars represent the mean ± SD (n = 3). (**F**) Construction of NS deletion mutants for SRSF3 binding site identification. (**G**) SRSF3 binding to NS deletion mutants in the absence of YTHDC1. A549-YTHDC1 knockout cells were transfected with plasmids containing either full-length NS or NS deletion mutants (#1 Mut and #2 Mut) for 48 h, followed by modified SRSF3-RIP-qPCR. Error bars represent the mean ± SD (n = 3). Statistical significance was determined using Student's t-test: ****P<0.0001. (**H**) Hypothetical model illustrating the competitive binding of YTHDC1 and SRSF3 on NS mRNA.

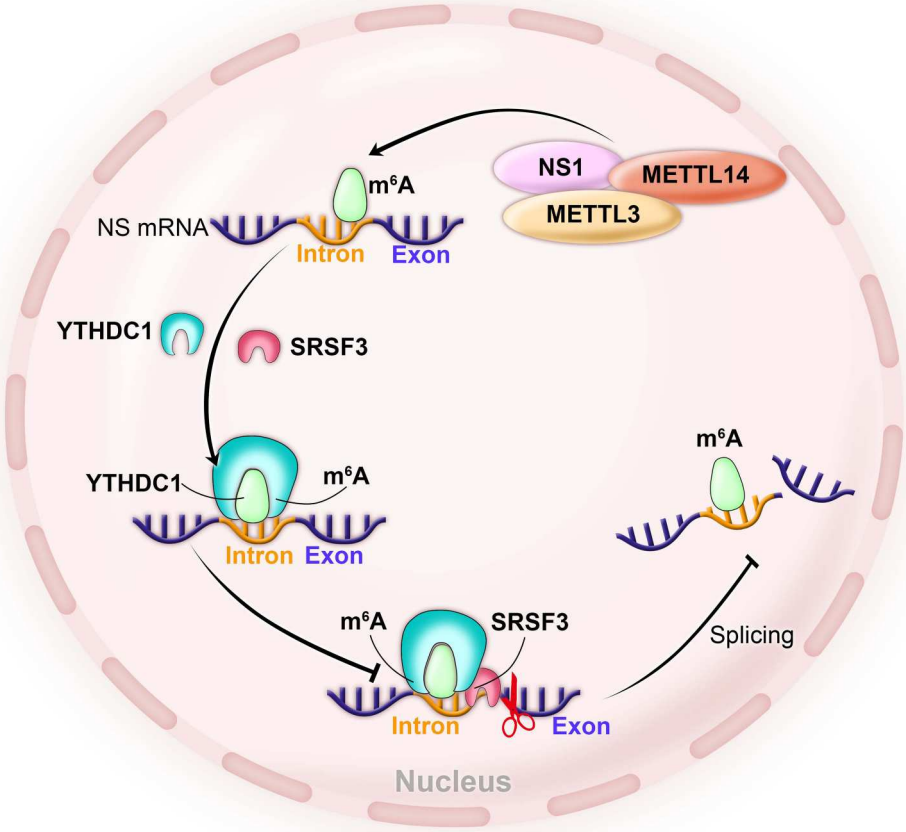

Figure 6. Working model describing NS1-mediated regulation of its own mRNA splicing via m^{6}A modification. Upon entry of NS mRNA into the nucleus, NS1 interacts with METTL3 and METTL14 to facilitate the m^{6}A addition on NS mRNA. The m^{6}A modification is then recognized by the m^{6}A reader YTHDC1, which blocks the association between NS mRNA and SRSF3, thereby suppressing splicing.

direction would lead to an unbalanced NEP/NS1 ratio, resulting in excessive NEP or NS1, either of which would reduce viral replication [38]. This negative feedback involves a strategic interaction in which NS1 initially recruits m^{6}A writers; however, at high concentrations, it saturates and inhibits their activity. Specifically, increasing levels of NS1 result in a marked decline in the interaction between METTL3 and NS mRNA, thereby directly reducing m^{6}A methylation. This dominant inhibitory effect on the m^{6}A writer machinery, rather than active recruitment of erasers, underpins the negative feedback loop that fine-tunes viral gene expression. Beyond splicing, nuclear export is another essential step in mRNA processing. While earlier studies reported that NS1 blocked nuclear export of its own mRNA in transfection systems [24, 30], △NS1 (NS1-deficient virus) infection experiments revealed that NS1 could promote M mRNA transportation from nucleus to cytoplasm [39]. The WSN/Ans1 model used here will be invaluable for further elucidating NS1′s role in regulating nuclear export of its own mRNA during bona fide viral infection.

Several m^{6}A modification sites on NS mRNA were identified through DRS analysis, with A385 specifically influencing NS mRNA splicing (Figure 3H). We identified another 8 nucleotides with the highest levels of m^{6}A modification through DRS and selected several of these sites for generation of targeted mutants to assess their roles in NS segment splicing (Figure S5A). The results showed that none of these other sites affected NS mRNA processing (Figure S5 B-C), suggesting that these sites may be involved in different viral functions. As previously mentioned, Zhu et al., reported that the PR8/A530C mutation negatively regulates NS mRNA splicing [17]. Notably, the A530 nucleotide precisely overlaps with the 3′ splice site, indicating a potential impact on NS mRNA splicing regardless of its chemical modification status. To further investigate this, we introduced an additional mutation (WSN/C531T) proximal to the 3′ splice site and compared the splicing ratio between WSN/C531T and WSN/WT to elucidate the underlying regulatory mechanisms. Notably, the splicing ratios of NS mRNA in WSN/C531 T and WSN/A530C infected cells were remarkably similar

(Figure S5 D-E). These findings strongly suggest that the m^{6}A modification might not be the primary factor influencing splicing efficiency in the WSN/A530C mutant.

Our results demonstrated that the regulatory influence of m^{6}A modification on NS mRNA splicing extends beyond the WSN (H1N1) strain, and is also observed in other influenza strains, including HK68 (H3N2), CA4 (H1N1), 1194 (H5N1), and GDV (H9N2). The conserved regulatory role of A385 is evident. Notably, in both mammalian and avian IAV-infected cells, m^{6}A modification was observed to negatively regulate NS mRNA splicing. However, in mammalian cells infected with the avian IAV strain, the regulatory effect of m^{6}A modification was observed to be less pronounced compared to avian cells infected with the same strain. Most cross-species transmission of IAV, particularly from birds to mammals, involves the exploitation of host factors, including m^{6}A -related proteins. m^{6}A modifications enable viral RNAs to evade immune sensors like RIG-I, promoting viral persistence [40, 41]. However, structural differences in methyltransferases between avian and mammalian hosts can hinder viral adaptation, as demonstrated by the GDV strain's differential m^{6}A regulation in human versus avian cells. Successful cross-species transmission thus requires viral evolution to optimize interactions with the host's m^{6}A machinery, which varies across species and shapes unique epitranscriptomic landscapes [42]. When an avian virus infects a mammal, it may acquire mutations in m^{6}A motifs or enhance interactions with host enzymes like METTL3 to sustain replication and evade immunity. This ongoing adaptation creates a feedback loop: viral modifications influence host m^{6}A systems, driving a co-evolutionary arms race. Similar mechanisms are observed in viruses such as KSHV and HIV, where manipulation of m^{6}A deposition facilitates infection [9, 43]. Altogether, these interactions highlight m^{6}A's dual role as both a mediator and marker of host–pathogen co-evolution, emphasizing that successful cross-species transmission hinges on the virus's capacity to adapt to the host's epitranscriptomic landscape.

In our study, we identified a highly conserved m^{6}A site (A385 on NS mRNA) that functionally regulates NS mRNA processing. Targeting this conserved m^{6}A site with selective inhibitors could potentially offer broad-spectrum activity across various IAV strains, provide a higher genetic barrier to the development of resistance compared to traditional protein-targeting antivirals, and incur minimal cytotoxic effects on host cells. This epitranscriptome-based approach represents a promising new therapeutic strategy capable of delivering robust protection against both seasonal influenza outbreaks and future pandemic threats.

The m^{6}A profiles of IAV described in this study performed exclusively in a cancer cell line. Sine RNA modifications are known to be cell type- and context-dependent [44, 45], further studies using primary human cells or animal models will be essential to validate the biological relevance of our proposed mechanism.

In summary, this study uncovers an uncharacterized epigenetic role for NS1 in inhibiting its own mRNA splicing, mediated by m^{6}A modification. We identified a conserved regulatory function for m^{6}A in NS mRNA processing, which suggests a universal mechanism influencing NS mRNA splicing in influenza A virus infections.

Acknowledgements

The authors are grateful to Dr. Jane Rayner for editing the manuscript. Nanopore-Based Direct RNA Sequencing was conducted by Wuhan Benagen Technology Co.

Author contributions

Conceptualization, Y.L., B.W-Y.M. and H.C.; Methodology, Y.L., B.W-Y.M., P.W. and J.L.; Acquisition of Data, Y.L., B.W-Y.M., P.W. and J.L.; Analysis and Interpretation of Data, Y.L. and B.W-Y.M.; Writing – Original Draft Preparation, Y.L. and B.W-Y.M.; Writing – Review & Editing, Y.L., B.W-Y.M. and H.C.

Disclosure statement

No potential conflict of interest was reported by the author(s).

Funding

This work was supported by Innovation and Technology Commission; Health@InnoHK, Innovation and Technology Commission; the Research Grants Council of the Hong Kong Special Administrative Region; The Government of the Hong Kong Special Administrative Region and Theme-Based Research Scheme: [grant number T11-709/21-N]; The Government of the Hong Kong Special Administrative Region; ITC funding support.

ORCID

Bobo Wing-Yee Mok http://orcid.org/0000-0003-3187-2736
Honglin Chen http://orcid.org/0000-0001-5108-8338

References

[1] Zhao BS, Roundtree IA, He C. Post-transcriptional gene regulation by mRNA modifications. Nat Rev Mol Cell Biol. 2017;18(1):31–42.
[2] Li S, Mason CE. The pivotal regulatory landscape of RNA modifications. Annu Rev Genomics Hum Genet. 2014;15:127–150.

[3] Meyer KD, Jaffrey SR. The dynamic epitranscriptome: N6-methyladenosine and gene expression control. Nat Rev Mol Cell Biol. 2014;15(5):313–326.
[4] Meyer KD, Saletore Y, Zumbo P, et al. Comprehensive analysis of mRNA methylation reveals enrichment in 3′ UTRs and near stop codons. Cell. 2012;149(7):1635–1646.
[5] Wang X, Feng J, Xue Y, et al. Structural basis of N(6)-adenosine methylation by the METTL3-METTL14 complex. Nature. 2016;534(7608):575–578.
[6] He L, Li H, Wu A, et al. Functions of N6-methyladenosine and its role in cancer. Mol Cancer. 2019;18(1):176.
[7] Paramasivam A, Priyadharsini JV, Raghunandhakumar S. Implications of m6A modification in autoimmune disorders. Cell Mol Immunol. 2020;17(5):550–551.
[8] Kennedy EM, Bogerd HP, Kornepati AV, et al. Posttranscriptional m(6)A editing of HIV-1 mRNAs enhances viral gene expression. Cell Host Microbe. 2016;19(5):675–685.
[9] Lichinchi G, Gao S, Saletore Y, et al. Dynamics of the human and viral m(6)A RNA methylomes during HIV-1 infection of T cells. Nat Microbiol. 2016;1:16011.
[10] Liu J, Xu YP, Li K, et al. The m(6)A methylome of SARS-CoV-2 in host cells. Cell Res. 2021;31(4):404–414.
[11] Chen J, Jin L, Wang Z, et al. N6-methyladenosine regulates PEDV replication and host gene expression. Virology. 2020;548:59–72.
[12] Lang F, Singh RK, Pei Y, et al. EBV epitranscriptome reprogramming by METTL14 is critical for viral-associated tumorigenesis. PLoS Pathog. 2019;15(6):e1007796.
[13] Krug RM, Morgan MA, Shatkin AJ. Influenza viral mRNA contains internal N6-methyladenosine and 5′-terminal 7-methylguanosine in cap structures. J Virol. 1976;20(1):45–53.
[14] Narayan P, Ayers DF, Rottman FM, et al. Unequal distribution of N6-methyladenosine in influenza virus mRNAs. Mol Cell Biol. 1987;7(4):1572–1575.
[15] Courtney DG, Kennedy EM, Dumm RE, et al. Epitranscriptomic enhancement of influenza A virus gene expression and replication. Cell Host Microbe. 2017;22(3):377–86.e5.
[16] Chen K, Luo GZ, He C. High-resolution mapping of N^6-methyladenosine in transcriptome and genome using a photo-crosslinking-assisted strategy. Methods Enzymol. 2015;560:161–185.
[17] Zhu Y, Wang R, Zou J, et al. N6-methyladenosine reader protein YTHDC1 regulates influenza A virus NS segment splicing and replication. PLoS Pathog. 2023;19(4):e1011305.
[18] Courtney DG. Post-transcriptional regulation of viral RNA through epitranscriptional modification. Cells. 2021;10(5):1129.
[19] Chen J, Wei X, Wang X, et al. TBK1-METTL3 axis facilitates antiviral immunity. Cell Rep. 2022;38(7):110373.
[20] Hale BG, Randall RE, Ortín J, et al. The multifunctional NS1 protein of influenza A viruses. J Gen Virol. 2008;89(Pt 10):2359–2376.
[21] Fortes P, Beloso A, Ortín J. Influenza virus NS1 protein inhibits pre-mRNA splicing and blocks mRNA nucleocytoplasmic transport. Embo j. 1994;13(3):704–712.
[22] Lu Y, Qian XY, Krug RM. The influenza virus NS1 protein: a novel inhibitor of pre-mRNA splicing. Genes Dev. 1994;8(15):1817–1828.
[23] Pleschka S, Jaskunas R, Engelhardt OG, et al. A plasmid-based reverse genetics system for influenza A virus. J Virol. 1996;70(6):4188–4192.
[24] Garaigorta U, Ortín J. Mutation analysis of a recombinant NS replicon shows that influenza virus NS1 protein blocks the splicing and nucleo-cytoplasmic transport of its own viral mRNA. Nucleic Acids Res. 2007;35(14):4573–4582.
[25] Robb NC, Jackson D, Vreede FT, et al. Splicing of influenza A virus NS1 mRNA is independent of the viral NS1 protein. J Gen Virol. 2010;91(Pt 9):2331–2340.
[26] Huang X, Zheng M, Wang P, et al. An NS-segment exonic splicing enhancer regulates influenza A virus replication in mammalian cells. Nat Commun. 2017;8:14751.
[27] Song W, Wang P, Mok BW, et al. The K526R substitution in viral protein PB2 enhances the effects of E627 K on influenza virus replication. Nat Commun. 2014;5:5509.
[28] Schägger H, von Jagow G. Tricine-sodium dodecyl sulfate-polyacrylamide gel electrophoresis for the separation of proteins in the range from 1 to 100 kDa. Anal Biochem. 1987;166(2):368–379.
[29] Conrad NK. Chapter 15. Co-immunoprecipitation techniques for assessing RNA-protein interactions in vivo. Methods Enzymol. 2008;449:317–342.
[30] Alonso-Caplen FV, Nemeroff ME, Qiu Y, et al. Nucleocytoplasmic transport: the influenza virus NS1 protein regulates the transport of spliced NS2 mRNA and its precursor NS1 mRNA. Genes Dev. 1992;6(2):255–267.
[31] Emeny JM, Morgan MJ. Regulation of the interferon system: evidence that vero cells have a genetic defect in interferon production. J Gen Virol. 1979;43(1):247–252.
[32] Paterson D, Fodor E. Emerging roles for the influenza A virus nuclear export protein (NEP). PLoS Pathog. 2012;8(12):e1003019.
[33] O'Neill RE, Talon J, Palese P. The influenza virus NEP (NS2 protein) mediates the nuclear export of viral ribonucleoproteins. Embo j. 1998;17(1):288–296.
[34] Xiao W, Adhikari S, Dahal U, et al. Nuclear m(6)A reader YTHDC1 regulates mRNA splicing. Mol Cell. 2016;61(4):507–519.
[35] Zheng M, Wang P, Song W, et al. An A14U substitution in the 3′ noncoding region of the M segment of viral RNA supports replication of influenza virus with an NS1 deletion by modulating alternative splicing of M segment mRNAs. J Virol. 2015;89(20):10273–10285.
[36] Sugimoto Y, König J, Hussain S, et al. Analysis of CLIP and iCLIP methods for nucleotide-resolution studies of protein-RNA interactions. Genome Biol. 2012;13(8):R67.
[37] Zhang C, Darnell RB. Mapping in vivo protein-RNA interactions at single-nucleotide resolution from HITS-CLIP data. Nat Biotechnol. 2011;29(7):607–614.
[38] Chua MA, Schmid S, Perez JT, et al. Influenza A virus utilizes suboptimal splicing to coordinate the timing of infection. Cell Rep. 2013;3(1):23–29.
[39] Mor A, White A, Zhang K, et al. Influenza virus mRNA trafficking through host nuclear speckles. Nat Microbiol. 2016;1(7):16069.

[40] Li H, Guo Y, Qi W, et al. N(6)-methyladenosine modification of viral RNA and its role during the recognition process of RIG-I-like receptors. Front Immunol. 2022;13:1031200.
[41] Qiu W, Zhang Q, Zhang R, et al. N(6)-methyladenosine RNA modification suppresses antiviral innate sensing pathways via reshaping double-stranded RNA. Nat Commun. 2021;12(1):1582.
[42] Bayoumi M, Rohaim MA, Munir M. Structural and virus regulatory insights into avian N6-methyladenosine (m6A) machinery. Front Cell Dev Biol. 2020;8:543.
[43] Tan B, Gao SJ. The RNA epitranscriptome of DNA viruses. J Virol. 2018;92(22.
[44] Wilkinson E, Cui YH, He YY. Roles of RNA modifications in diverse cellular functions. Front Cell Dev Biol. 2022;10:828683.
[45] Chen D, Gu X, Nurzat Y, et al. Writers, readers, and erasers RNA modifications and drug resistance in cancer. Mol Cancer. 2024;23(1):178.